

See discussions, stats, and author profiles for this publication at: <https://www.researchgate.net/publication/265139871>

Toward an Autonomous Sailing Boat

Article in IEEE Journal of Oceanic Engineering · April 2015

DOI: 10.1109/JOE.2014.2321714

CITATIONS

29

READS

9,127

5 authors, including:



Frederic Plumet

Sorbonne Université

53 PUBLICATIONS 687 CITATIONS

[SEE PROFILE](#)



Clement Petres

Sorbonne Université

12 PUBLICATIONS 559 CITATIONS

[SEE PROFILE](#)



Sio-Hoi leng

Sorbonne Université

92 PUBLICATIONS 2,041 CITATIONS

[SEE PROFILE](#)

Towards an Autonomous Sailing Boat

Frédéric Plumet,

Clément Pêtrès, Miguel-Angel Romero-Ramirez, Bruno Gas, Sio-Hoi Ieng

Abstract

Among autonomous surface vehicles, sailing robotics could be a promising technology for long term missions and semi-persistent presence in the oceans. Autonomy of such vehicles in terms of energy will be achieved by renewable solar and wind power sources. Autonomy in terms of sailing decision will be achieved by innovative perception and navigation modules. The main contribution of this paper is to propose a complete hardware and software architecture for an autonomous sailing robot. The hardware architecture includes a comprehensive set of sensors and actuators as well as a solar panel and a wind turbine. For obstacle detection, a segmentation is performed on data coming from an omnidirectional camera coupled with an inertial measurement unit and a sonar. For navigation and control of the vehicle, a potential based reactive path planning approach is proposed. The specific sailboat kinematic constraints are turned into virtual obstacles to compute a feasible and optimal heading in terms of cost of gybe and tack maneuver as well as safety relative to obstacle danger. Finally, field test experiments are presented to validate the various components of the system.

Index Terms

Marine robotics, autonomous sailing robot, omnidirectional vision, obstacle avoidance, reactive path planning.

I. INTRODUCTION

During the recent years, one can note a growing activity concerning the use of autonomous surface vehicles (ASV) with applications such that port protection, mines countermeasure, recon-

This work was supported by the ANR project ASAROME (Num. ANR-07-ROBO-0009).

Sio-Hoi Ieng is with The Vision Institut, UPMC Univ Paris 06, UMR 7210, 4 place Jussieu, 75005 Paris - France. E-mail: ieng@upmc.fr

All other authors are with the Institute for Intelligent Systems and Robotics (ISIR), UPMC Univ Paris 06, CNRS - UMR 7222, 4 place Jussieu, 75005 Paris - France. E-mails: lastname@isir.upmc.fr

naissance and surveillance mission [1]–[3]. One of the probably most important reason that can explains this growing activity is the need for better environmental monitoring. Meteorological and ecological studies in particular need better characterization of the global Earth's processes and consequently requires a broad spectrum of observational tools to understand the complex interactions between the oceans and the atmosphere.

Ocean sensing have been typically done with satellites, airplanes, buoys, research vessels or ships of opportunity. However, satellites and airplanes are limited by cloud cover, temporal/geographical coverage as well as spatial resolution. Manned research vessels are expensive to deploy and usually suffer from a weak of availability. Spatial sampling is impossible with moored buoys and they cannot be self-deployed to specific areas of interest. Over the last decades, the growing needs of the oceanographic community for in-situ measurements and complementary observing systems have stimulated the robotic community of academic researchers and private companies. Thus, considerable progress have been observed in the development and use of autonomous marine platforms such as drifters, gliders, autonomous underwater vehicles (AUV), and autonomous surface vehicles.

Each of these platforms provides various capabilities for payload, communication, mobility, and autonomy. In the recent years, numerous ASV have been developed for bathymetric data recording in shallow water [4], monitoring of various marine environmental data either alone [5]–[7] or as part of a sensor network [8]–[12]. All of these aforementioned vehicles are conventional electric powered systems and suffer from a lack of autonomy that restrains their usage to short term missions. Sailing robots could be an efficient solution for long term missions and semi-persistent presence in the oceans since they rely on renewable energy like solar and wind energies [13], [14]. However, a complete and operational hardware architecture for building a reliable autonomous sailing system is still a challenge. A software architecture able to provide fully autonomous cognition capabilities is also an issue.

The main contribution of this paper is to propose a complete hardware and software architecture, which has been developed in the framework of the Autonomous SAiling Robot for Oceanographic MEasurements (ASAROME) project. The hardware architecture includes a comprehensive set of sensors and actuators powered by a battery pack that is charged by a solar panel and a wind turbine. For obstacle detection, a segmentation is performed on data coming from an omnidirectional camera coupled with an inertial measurement unit (IMU) and a sonar.

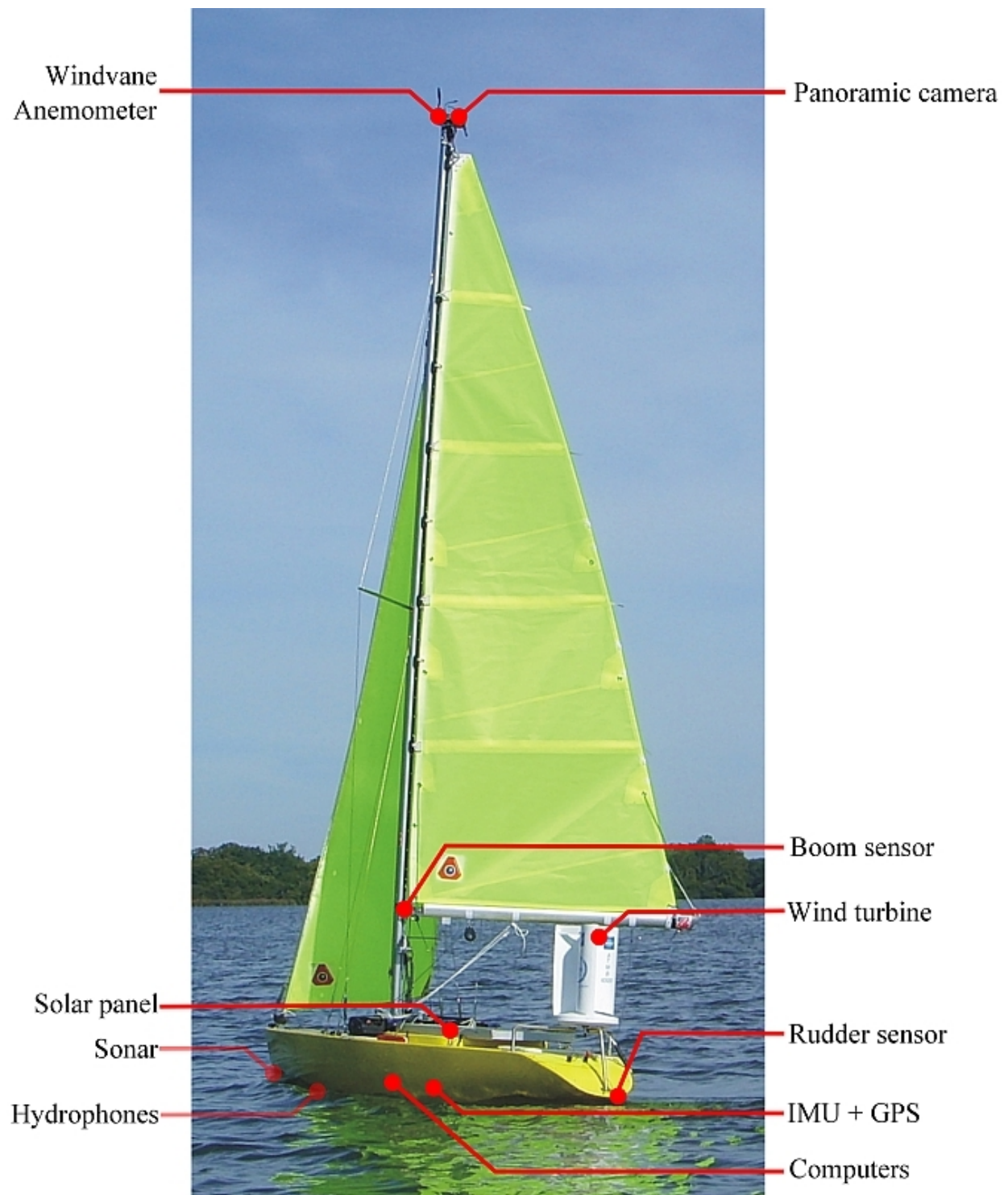


Fig. 1. The sailboat prototype of the ASAROME project

For navigation and control of the vehicle, a potential based reactive path planning approach is proposed. The specific sailboat kinematic constraints are turned into virtual obstacles to compute a feasible and optimal heading in terms of travel time, cost of gybe and tack manoeuvres as well as safety relative to obstacle danger.

The paper is organized as follows. First, the hardware architecture of our prototype is presented. Sensors, actuators and computers are described as well as the communication links between them. Second, the perception module, including data fusion and segmentation processes, is presented. Third, the navigation and control module are described. The path planning algorithm reacts to changes of the wind conditions as well as detected obstacles in real-time by recalculating the heading periodically. This method has been successfully tested under various wind conditions using a dedicated numerical simulator as well as actual field trials.

II. SAILING BOAT ARCHITECTURE

Autonomous navigation of robotic sailboats in dynamic and unknown environments is a challenging task, requiring reliable hardware and software architectures. The hardware architecture includes a wide range of sensors, three embedded computers and a set of actuators for rudder control and mainsail tuning.

A. Hardware architecture

An overview of the hardware architecture is illustrated in Fig. 1 and described in Fig. 2 with the following functional division: red blocks for perception, green blocks for actuation, blue for navigation and white blocks for internal and external communication.

1) Sensors and actuators: The perception of the environment is performed by a panoramic camera (Prosilica IP Camera GE1350C), a sonar (Tritech Micron) and a pair of hydrophones (Aquarian H2a) for obstacle detection and by a windvane-anemometer (Rowind CV3F) for wind speed and direction observations. The knowledge of the internal state of the system is assured by a low-cost MEMS based IMU combined with a GPS receiver (Xsens MTi-G) for global positioning and attitude monitoring. For boom angle, an absolute encoder is used (Hermetic Baumer Absolute Encoder). Current speed is sensed using a water speed sensor (Furuno SP235TR-2).

For actuation of the sailboat, rudder and boom angles are trimmed by the low level controller. In our prototype the rudder is actuated by a linear electric jack (Linak LA12-300N with an

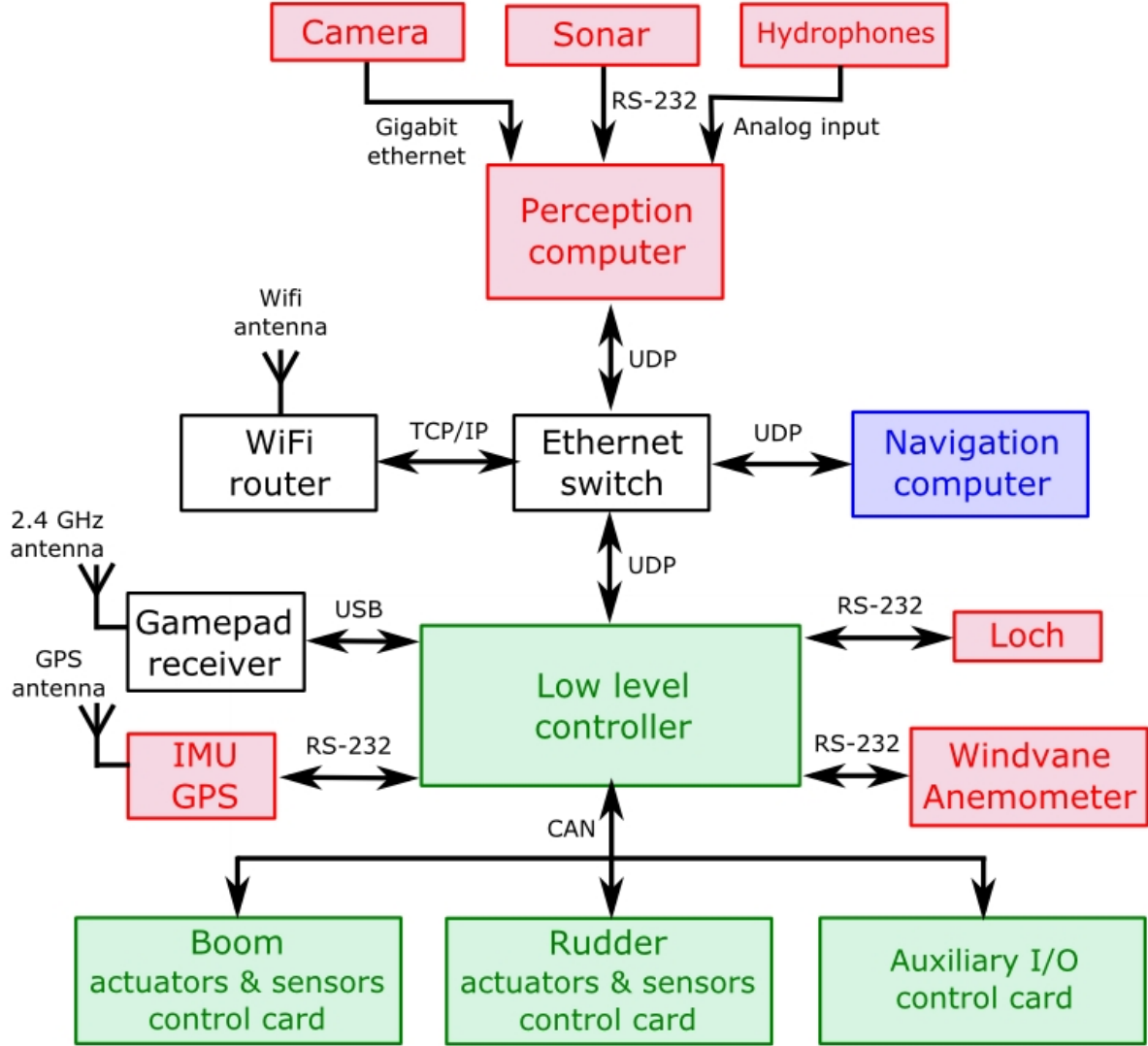


Fig. 2. Hardware architecture

integrated position sensor) and the boom by an electric fishing reel (Kristal fishing XL630) through non-reversible mechanisms in order to limit the electrical power consumption when not in use. A set of auxiliary inputs and outputs are reserved for side light management, emergency buttons and other safety functionalities.

2) *On-board computers:* For cognition tasks, one computer is dedicated for each of the following modules, perception, navigation and control. The perception module is the most demanding process of our system in terms of computational resources. A Arbor mini ITX

PC Box with an embedded Atom N270 processor is dedicated to these data acquisition and data fusion tasks. A Lippert PC-104 with an Atom N270 processor is used for the navigation task. The low level controller is based on an Emtrion embedded case module with a Renesas SH7781@400 MHz processor.

3) Communication: An UDP protocol has been designed with the aim of providing flexible bidirectional data transfer between the three embedded computers via a simple Ethernet switch. Sensors and actuators have different communication protocols depending on firmware implementations, such as gigabit Ethernet, RS-232, CAN and USB protocols. A manual control of the boat remains possible via a wireless link, using whether a gamepad or a remote computer.

4) Power sources and energy balance: Solar energy will be captured using a 0.5 m^2 solar panel (Sunset AS60, 60W-17.9V) able to deliver up to 60 W under maximal lighting conditions. Wind energy is captured using a wind turbine (Atmb 1000 50W-12V) able to deliver about 10 W for a wind speed of 10 knots. Regulation of the electric flow is done by a battery pack (12 V, 120 Ah) located in the keel of the boat. Under typical weather conditions in Western Europe, the two aforementioned power sources deliver about 35 W in average. On the basis of a full time operation of the embedded computers and sensors an average time usage of 20% of the rudder actuator and 10% of the sail actuator, the harvested power combined with the battery pack leads to two days of energetic autonomy. This limited autonomy is sufficient for short field trials of our prototype. However, for long-term missions a better power budget will be necessary.

B. Software architecture

An overview of the software architecture is shown in Fig. 3. Within the framework of this work, it is assumed that the mission planning task has previously been performed and that a list of way points $\{W_p\}$ has already been selected by an human mission planner or computed by a commercially available software.

A perception module gets the data from the system and from the environment to feed back the navigation and control modules with an updated representation of the internal state of the system and the external state of the world as well as an updated version of the map, including new detected obstacles.

The navigation module, which runs a local path planning algorithm, computes in real time a feasible heading as well as a sail angle to reach the current way points while avoiding obstacles.

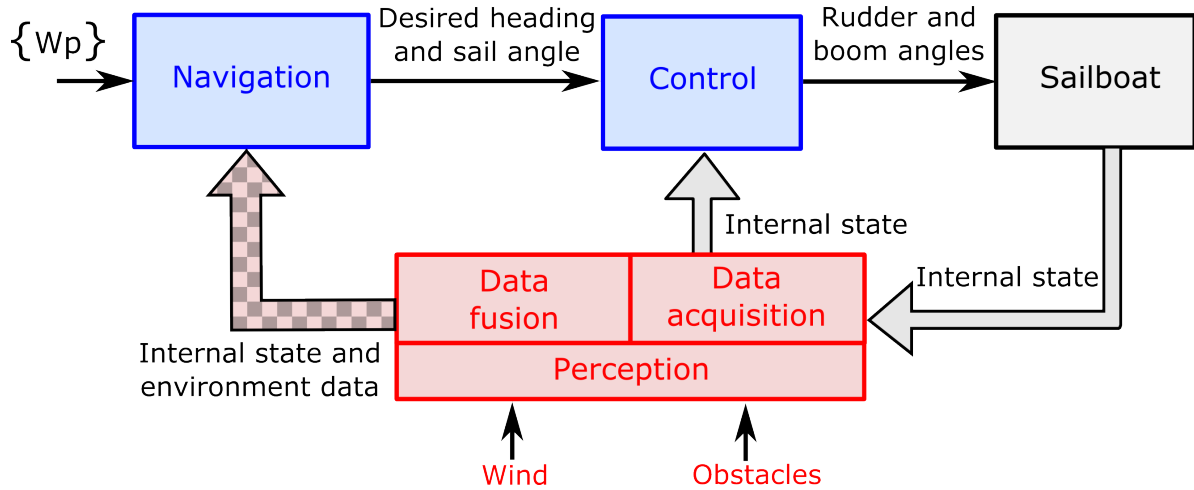


Fig. 3. Software architecture

1) Perception module: Sensor data include wind speed and direction, position and attitude of the boat, visual and acoustic data. These sensors have different acquisition frequencies, different spatial distributions and resolutions. First, collecting and formatting all the input data from the sensors is necessary and carried out by the data acquisition subsystem within the perception module. Each data is timestamped using a common clock in order to have a coherent dating of all the measurements. Second, a map of the environment is built to feed the navigation module. The main issue at this stage is to reliably detect and localize the obstacles. See section III for more details about data analysis considerations.

2) Navigation module: The role of the navigation module is to supply, in real time, the control system with a heading reference and a desired sail angle.

The heading is computed using a reactive path planning algorithm, which computes a new heading reference at each refresh of the data coming from the perception module. The path planning algorithm is described in details in section IV. Basically, it computes an optimal heading for the boat in the sense of a cost function including criteria such as cost of maneuvers and safety relative to obstacle danger.

For the computation of the sail angle, we use an adaptation of the method described in [15] to

the particular design of the mainsail.

3) Control module: The desired heading and sail angle, coming from the navigation module, are used as reference for this low level control module. The sail control is straightforward since the sail angle is directly measured by an internal sensor and controlled by electric actuator and a rope system. For the rudder control, a simple proportional-derivative controller is designed based on the heading error. The current heading of the sailboat is measured in real time by the IMU-GPS sensor. This PD control loop will react to environmental disturbances, such as waves or water currents and wind shifts that may affect the course of the boat.

4) Sailboat simulator: Before migration of the software on our prototype, a numerical simulator of the real sailboat can been used to test and validate the navigation and control algorithms. In this simulator, which integrates the differential equations of motion, both aero and hydrodynamic forces acting on the sailboat are taken into account (see [16] for further details).

Using this numerical simulator of our sailboat, a speed polar diagram can also be computed (see Fig. 4). These performance curves correspond to the steady-state maximum velocity of the vehicle for a given wind speed and a given wind direction and for headings φ relative to the wind direction varying from 45° to 315° .

For wind speeds varying from 5 to 20 knots, speed profiles look similar. A so-called *upwind no-go zone* is discarded for $-45^\circ \leq \varphi \leq 45^\circ$. Another forbidden sailing zone, called *downwind no-go zone*, is also exhibited for $150^\circ \leq \varphi \leq 210^\circ$. In fact, the boat is able to navigate in this region, but for safety reasons (instability) these headings will also be avoided in practice. These speed polar diagram and no-go zones will be used by the local path planning algorithm (see Section IV Navigation).

III. PERCEPTION

Data collected from embedded sensors are relative to the specific frames of these sensors. The relation between the sensors frames and the boat frame R_b is supposed to be known as well as the relation between R_b and a global reference frame R_w related to the Earth, thanks to the embedded IMU-GPS sensor.

For world modeling and obstacle detection, two sensors are used in our system: an omnidirectional camera and a sonar (see for example [17]–[21] among many others). The camera provides

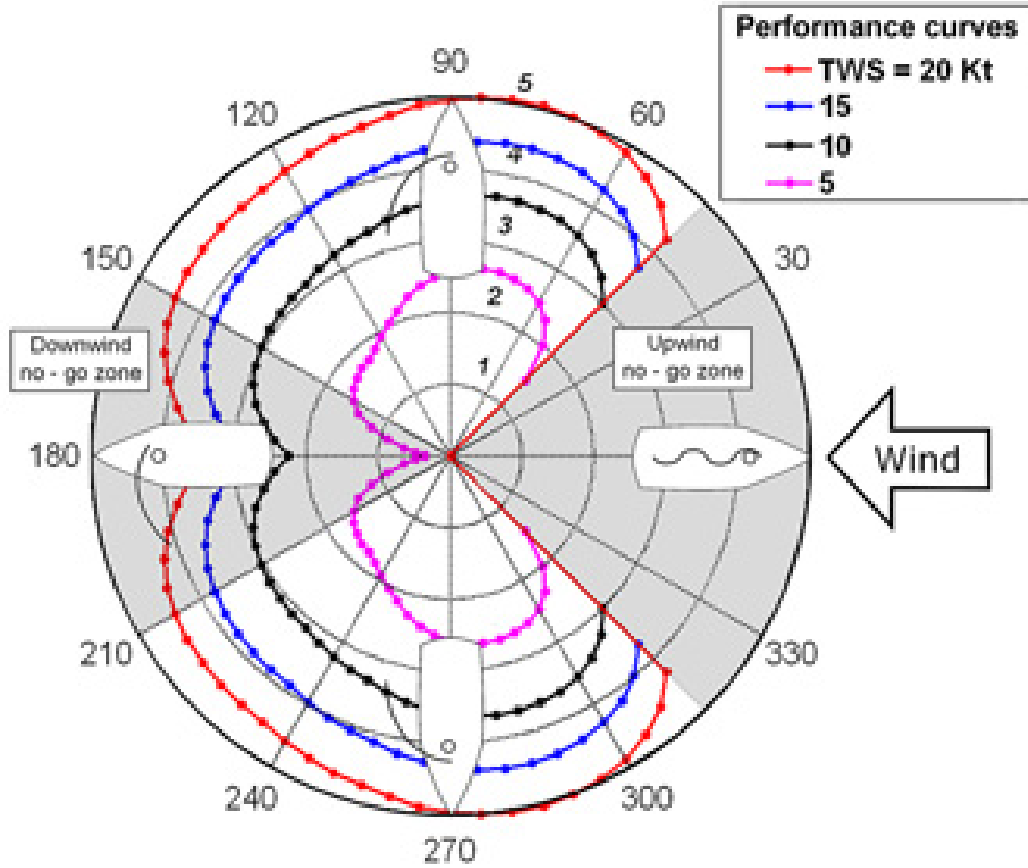


Fig. 4. Speed polar diagram of the sailboat

high rate and high resolution images of the water surface around the boat for distances up to the skyline (see Fig. 5 for an example of a panoramic view). The sonar provides low rate and low resolution images of the marine environment below the surface of the water in the vicinity of the boat. These two sensors are complementary as we will see in this section.

A. Visual sensor

The waterproof panoramic camera used in our sailing boat prototype is a compound system made of a high quality camera, a convex mirror and a transparent acrylic tube (see Fig. 6). For referencing visual data to the boat reference frame, a calibration of the vision system is necessary. Once a relation between objects in the scene and points in the image has been defined, an obstacle detection and localization algorithm can be used to feed the navigation module.

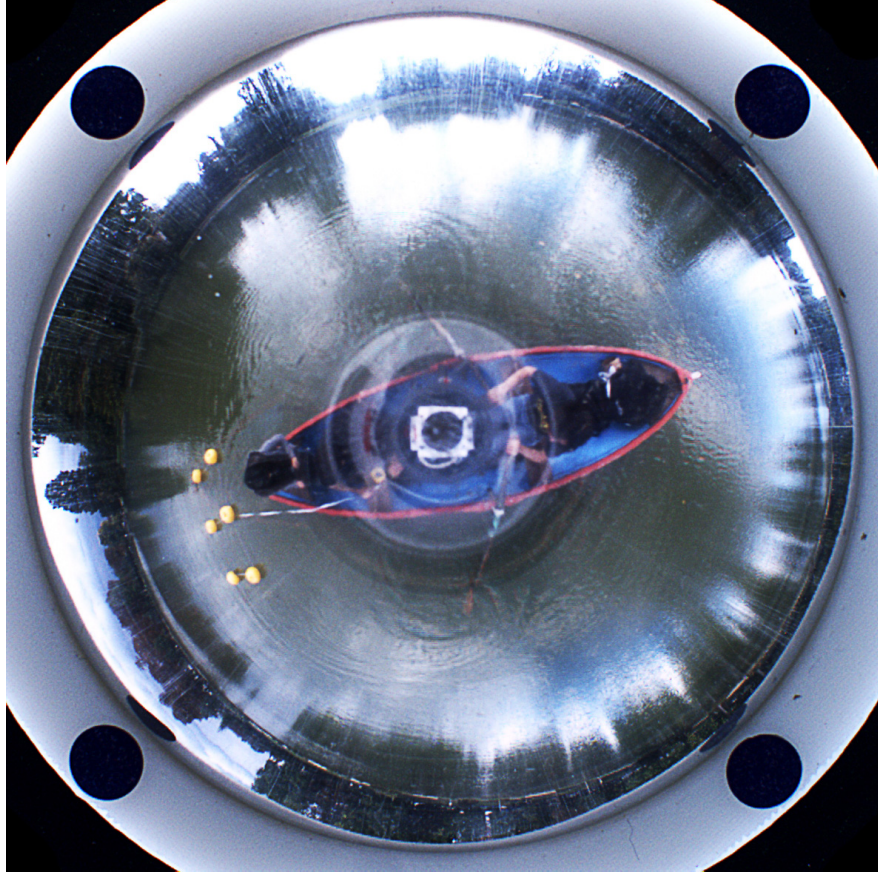


Fig. 5. An example of panoramic view. In this experiment the camera is fixed at the top of a 2.25 m mast

1) *Camera calibration:* The calibration process aims at determining the correspondence between a pixel p_i in the image to a point P_i in the world. The intrinsic parameters of the camera, the surface of the mirror and the refraction properties of the tube are first to be determined using the method described in [22]. Second, a ray (m_i, u_i) in the camera referenced frame R_c is constructed (see Fig. 7). Third, knowing the relation between R_c and the world reference frame R_w via the boat referenced frame R_b , the intersection between (m_i, u_i) and the sea surface gives P_i . Note that the sea surface is assumed to be calm in this framework.

2) *Obstacle detection:* The obstacle detection is done in two steps. First, an image difference between two consecutive images is performed to extract a coarse position of moving objects considered as potential obstacles. These areas of interest will be processed in the second step of the algorithm, which is based on a colorimetric criteria. According to the natural conditions, the color of the sea surface may be different from the color of the obstacles. This is the reason

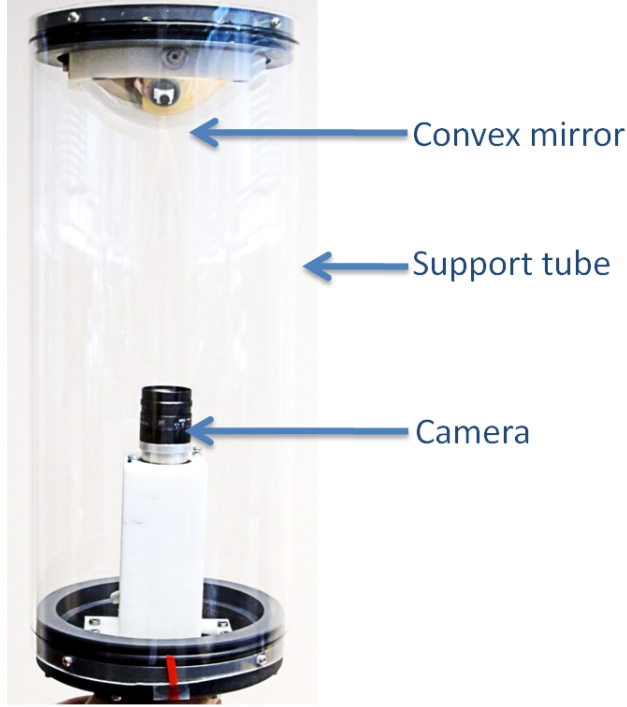


Fig. 6. The panoramic camera fixed at the top of the mast of the prototype

why the colorimetric criteria described in [22] is used for addressing the obstacle detection and localization issues.

B. Acoustic sensor

A Tritech Micron DST Sonar will be used on our sailboat prototype and is intended to be fixed under the keel, around 1.5 m beneath the waterline. This CHIRP (Compressed High Intensity Radar Pulse) sonar has a theoretical spatial resolution of 7.5 mm, a range settings from 2 m to 200 m and an horizontal beamwidth of 3°.

For obstacle detection, a very simple filtering technique is used: all the data under a given power threshold and a given size are discarded. The detected obstacles consist of the remaining set of "pixel". On these sets, the centroid of each detected obstacle can be computed as well as its estimated length.

Fig. 8 shows an example of an experimental sonar record. For this record, the sonar is 60 cm beneath the surface, its range has been set to 20 m, the angular resolution to 2° and the scanned

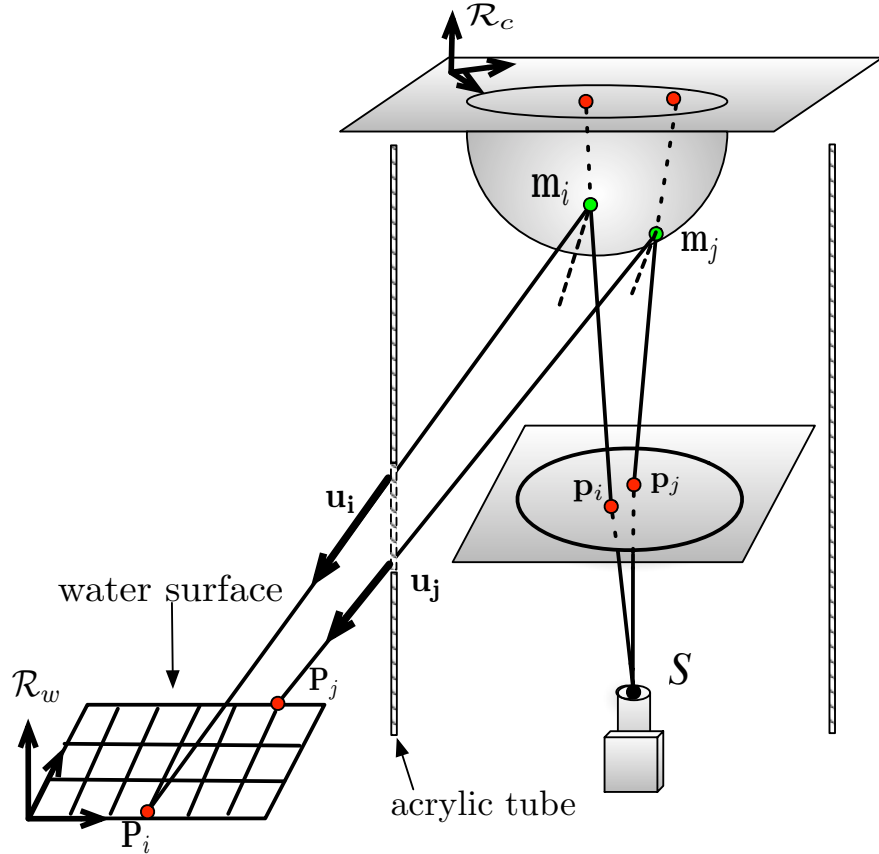


Fig. 7. Scheme of the omnidirectional camera and correspondence between a pixel p_i in the image and a point P_i in the world.

angular sector is from -90° to $+90^\circ$. A scan of the half plane lasts 5 seconds. The only obstacle in this case (a 80 cm reflective panel) is detected on the lower right part of the figure.

C. Data analysis

In this section, a set of experiments is presented to analyze the appropriateness of using both visual data (from the camera) and acoustic data (from the sonar) for obstacles detection and localization.

These experiments were conducted on a lake, on the surface of which a particular buoy has been anchored. The upper part of the buoy (50 cm large) is colored in yellow, the submerged part is the deflective panel described above. The panoramic camera was fixed on top of a tripod of 2.25 m height on a rowing boat.

A set of measures has been performed for distances of the buoy from the platform varying

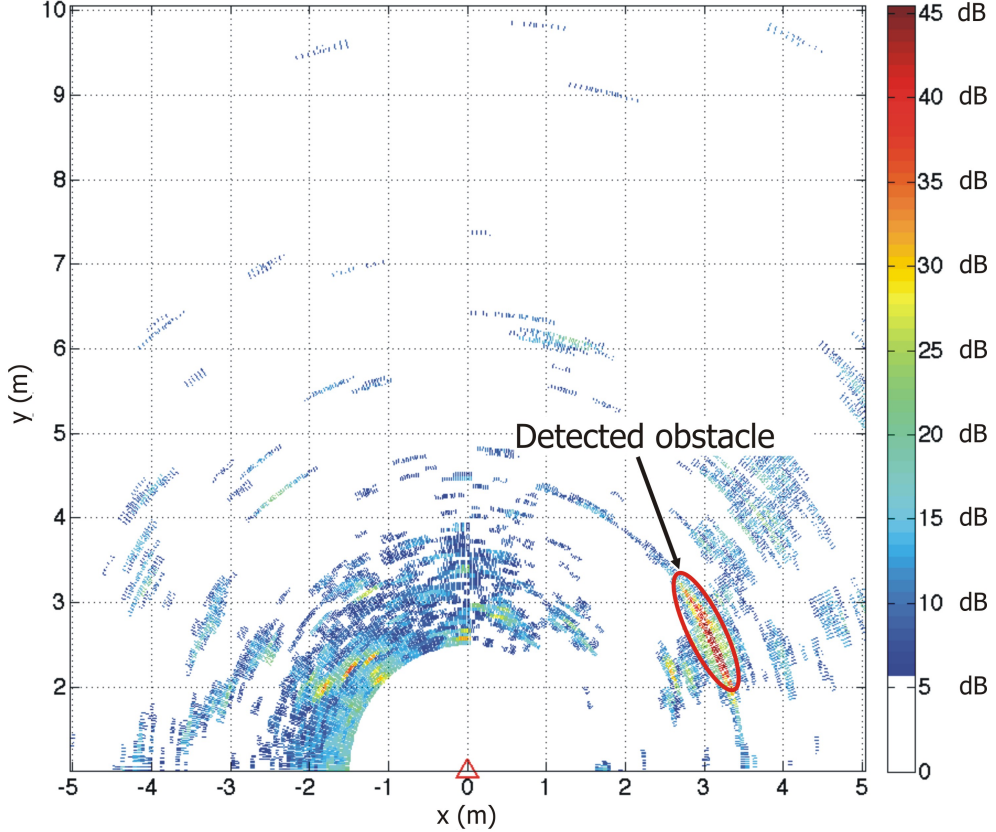


Fig. 8. Illustration of a significant sonar echo of a submerged obstacle

between 4 m and 16 m with a 180-degree scanning sector for the sonar.

As mentioned earlier, visual and acoustic data are dated. The camera generates 15 frames per second. The sonar produces an image every 5 seconds, however the time t and the distance d corresponding to a sonar angle a can be determined. For each angle a_i corresponding to a detected obstacle at time t_i , the sonar estimated distance d_i is compared to the camera estimated distance from the frame grabbed at the closest time to t_i .

Visual and acoustic data appear to be complementary, as depicted in Fig. 9 (a) and (b). We propose to apply a simple data fusion algorithm that averages distances from both sensors after an out-layer pre-processing.

Fig. 9 (a) depicts estimated distances using visual and acoustic sensors independently. In this case a simple average of the measures improves the estimated distance accuracy, as depicted in Fig. 9 (c). Fig. 9 (b) depicts both sets of data in presence of out-layers in the visual data

set. In this case, a comparison made on each modality between current and previous estimated distances is sufficient to detect and discard the most probable out-layer candidates. The average processing is then done as previously, and depicted in Fig. 9 (d).

These preliminary results show that it is appropriate to consider a multisensor data fusion method. In the case of vision for example, temporary bad lighting conditions can cause errors generation. The data fusion will then improve the robustness of the estimates. The main reason is that submerged obstacles can not be detected by any aerial visual device, and conversely. Finally, it should be noted that these experiments were conducted under static conditions. In the more general case of a moving platform, it will be necessary to consider a system taking the motion of the platform into account, by using for instance an adaptive Kalman based estimator.

IV. NAVIGATION

In the recent years, numerous methods have been proposed for the path planning of autonomous sailboats: based on implementation of classical sailing methods (such as Velocity Made Good, for example) [23], [24], state machine [25]–[27], fuzzy or neural control [28], [29] or ray-tracing techniques [30]. Potential field methods, due to Khatib [31] and Krogh [32], have been successfully employed for robot control and motion planning of mobile robots (see for example [33]–[36] among many others) and was adapted for the first time by authors for autonomous sailing boats in [16].

A. Local path planning using potential field

In classical artificial potential fields methods, the motion of a robot is governed by a field with two main components: an attractive potential driving the robot towards the goal and a repulsive potential pushing the robot away from obstacles. In order to adapt this method to the particular behavior of a sailboat, the main idea consists of adding a virtual obstacle around the boat to represent the so-called upwind and downwind no-go zones (see illustration Fig. 10). An hysteresis potential is also introduced to take into account the cost of tacking (turning the bow to the wind) and gybing (turning the stern to the wind) maneuvers. This hysteresis potential makes our method easy to tune according to the vehicle or mission specifications.

One of the main advantage of this potential field approach is that it provides a unified framework to represent all the components involved in the navigation process: goal and obstacle

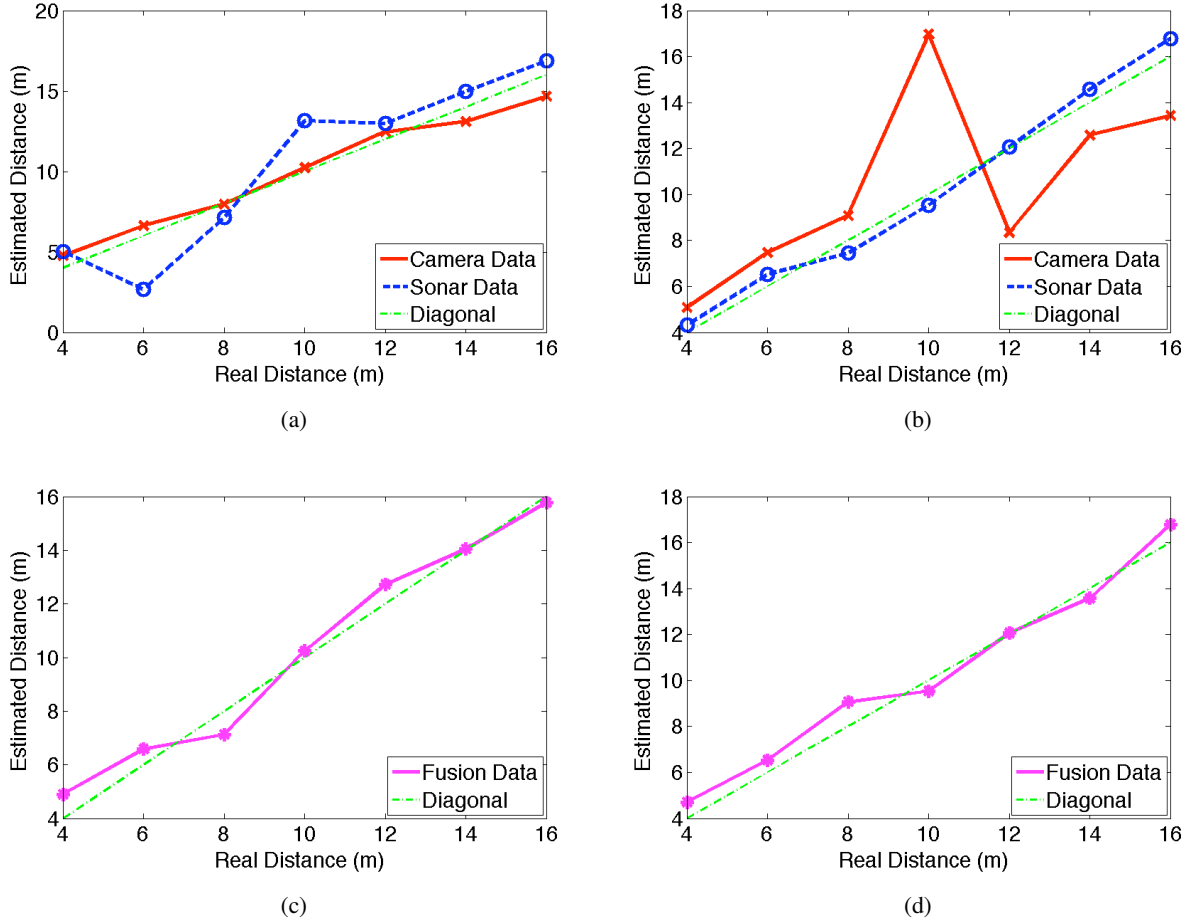


Fig. 9. (a) Sonar and camera estimated distances. (b) Sonar and camera estimated distances in presence of out-layers in camera data. (c) and (d) Estimated distances after treatment of (a) and (b) data respectively

locations, speed characteristics of the boat, costs of tack and gybe maneuvers and danger of obstacles are all taken into account by an attractive or a repulsive potential.

A major drawback with potential field techniques is their susceptibility to local minima but, for oceans monitoring missions, this risk will not be considered as an issue here because, in one hand, a global path planning is performed first to define way points far away from the shore of known obstacles (coast, island) and on the other hand, the marine environment is very sparse compared to classical indoor robotics environment (obstacles are other boats or drifting objects).

From a computational point of view, the potential fields path planning method is very fast and reliable since it requires only a summation of the different fields associated with the goal

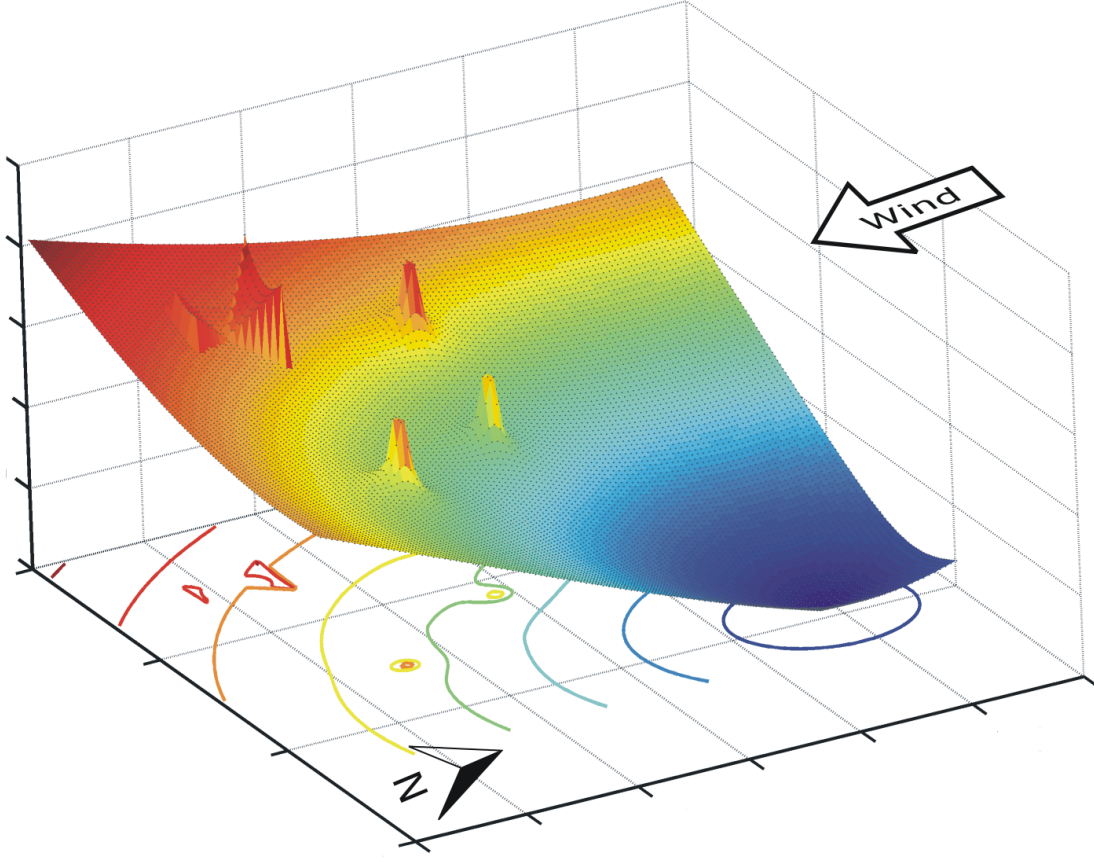


Fig. 10. Illustration of the potential relative to three obstacles and to a goal point located at the North-East corner of the map

U_g , with each obstacles $U_o^{(j)}$ and with the wind U_w :

$$U = U_g + \sum_j U_o^{(j)} + U_w$$

In practice, this overall potential is computed at each sampling time but only along a ring centered in the current boat position. The desired heading for the next move is the angle corresponding to the global minimum of the profile.

The attractive potential U_g associated with the goal (the current way point) is defined by:

$$U_g = G_g d_g$$

where G_g is a constant weighting factor and d_g the Euclidean distance between the boat position P and the current way point position P_g .

In the same way, the repulsive potential $U_o^{(j)}$ can be computed for each obstacle j :

$$U_o^{(j)} = \begin{cases} G_o \left(\frac{1}{d_o^{(j)}} - \frac{1}{d_{inf}} \right) & \text{if } d_o^{(j)} \leq d_{inf} \\ 0 & \text{otherwise} \end{cases}$$

where G_o is a constant weighting factor, $d_o^{(j)}$ is the Euclidean distance between the boat position P and the obstacle position $P_o^{(j)}$ and d_{inf} the distance of influence of the obstacle. This potential tends toward infinite when the vehicle is close to the obstacle to avoid any collision. The list of detected obstacle is periodically updated by the on-board perception module.

Finally, a virtual, wind-dependent obstacle and its related (repulsive) potential U_w is also introduced in order to encompass the specific kinematic of the sailboat (see illustration Fig. 11). This potential, based on the specific speed polar diagram of the sailboat, is moving with the vehicle and updated in real time, according to changes of wind speed and direction.

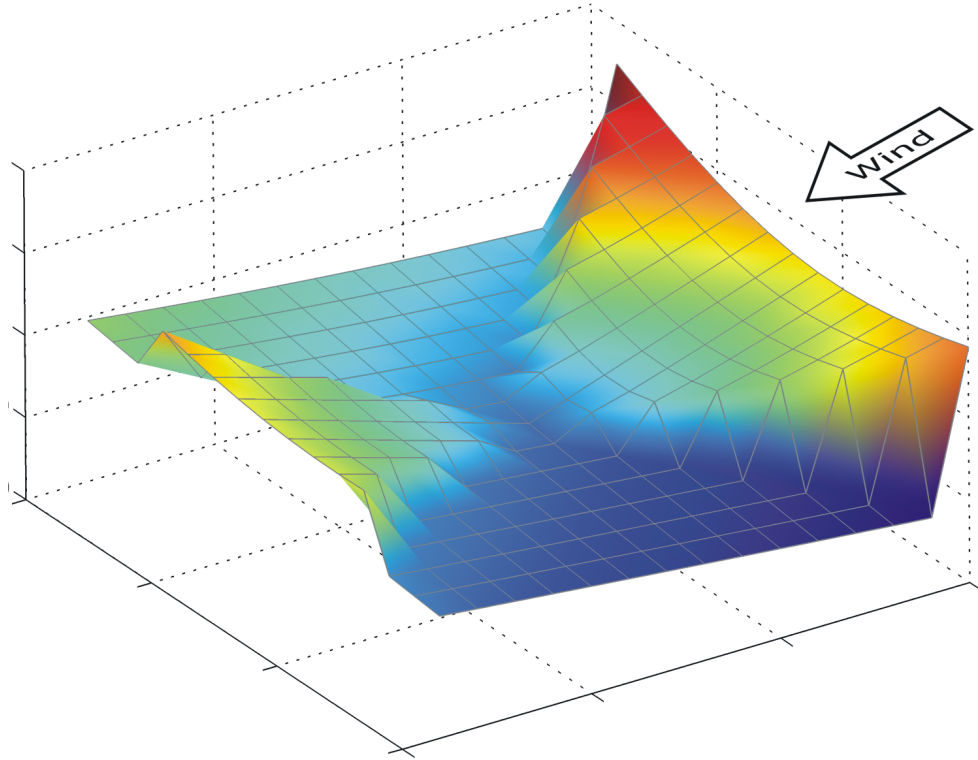


Fig. 11. Close-up on the repulsive potential built around the boat: upwind/downwind virtual obstacles and hysteresis potential

This wind potential U_w around the boat is defined by:

$$U_w = \begin{cases} P_{ngz} & \text{if } \phi \in [\text{no-go zone}] \\ P_h + G_v \frac{V - V_{max}}{V_{max}} & \text{otherwise} \end{cases}$$

with V the current sailboat velocity, V_{max} the estimated maximal velocity (for the current wind speed) and G_v a constant weighting factor. P_{ngz} is the constant (high) value of the potential associated to the upwind and downwind no-go zones (see Fig. 12, where for the sake of simplicity, the speed polar diagram is assumed to be ideal and represented by the dotted circle).

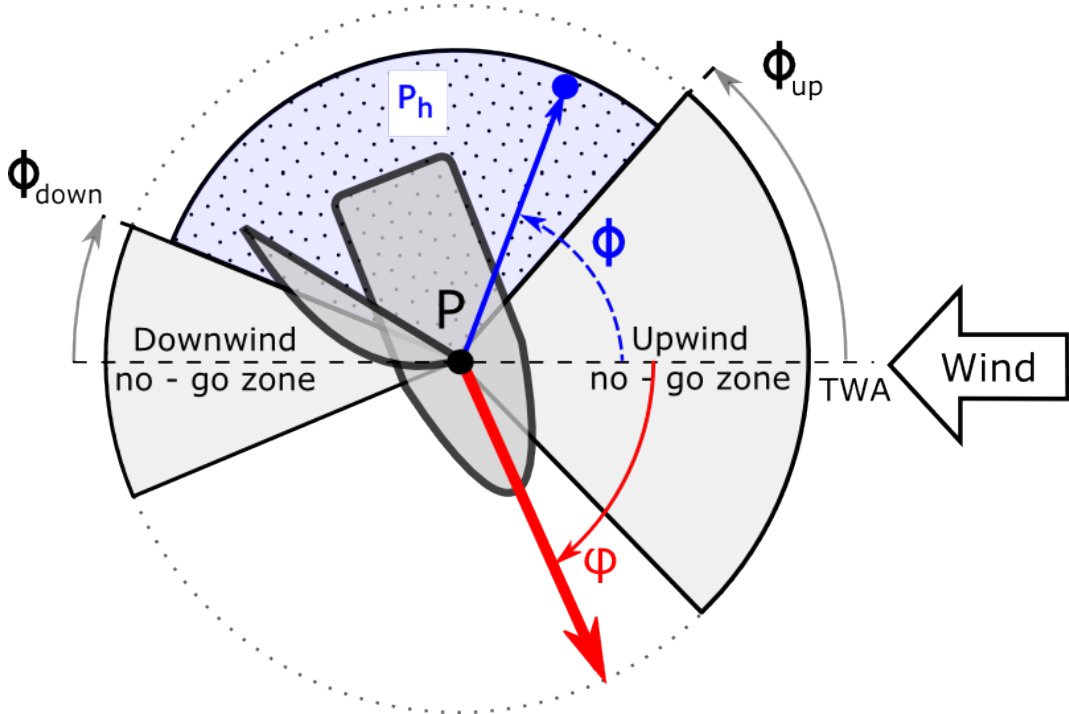


Fig. 12. Scheme of the upwind and downwind no-go zones. The dotted area corresponds to the region where $P_h \neq 0$

The so-called hysteresis potential P_h is introduced here to prevent the sailboat from tacking or gybing too frequently. P_h is equal to zero if ϕ is in the same half plane as the current heading φ (with respect to the wind) and is set to a positive value otherwise. This way, only one parameter has to be set up to fit the cost of gybing and tacking into account. In fact, this parameter can be used to control the number of maneuvers when navigating directly upwind or downwind: if this parameter is set to a high value, the number of maneuvers will be small but conversely the sailboat will move far away from the straight line between two way points. It can thus also

be used to meet the missions requirements, especially when the boat has to navigate in narrow channel between islands for example.

Before implementing this algorithm on the real sailboat, simulation have been performed using the sailboat simulator to test the algorithm and tune the different parameters. Obstacle avoidance as well as influence of the hysteresis potential are illustrated figure 13 for abeam navigation with a constant wind (speed and direction). In this case, the way point is located directly upwind and the sailboat still reach the goal while avoiding obstacles. The results for three different hysteresis values are depicted figure 13: the red trajectory has been computed with $P_h = 3$, the blue trajectory has been computed with $P_h = 2$ and the black trajectory has been computed with $P_h = 1$. Two, three and seven tacks have been respectively executed to reach the goal point.

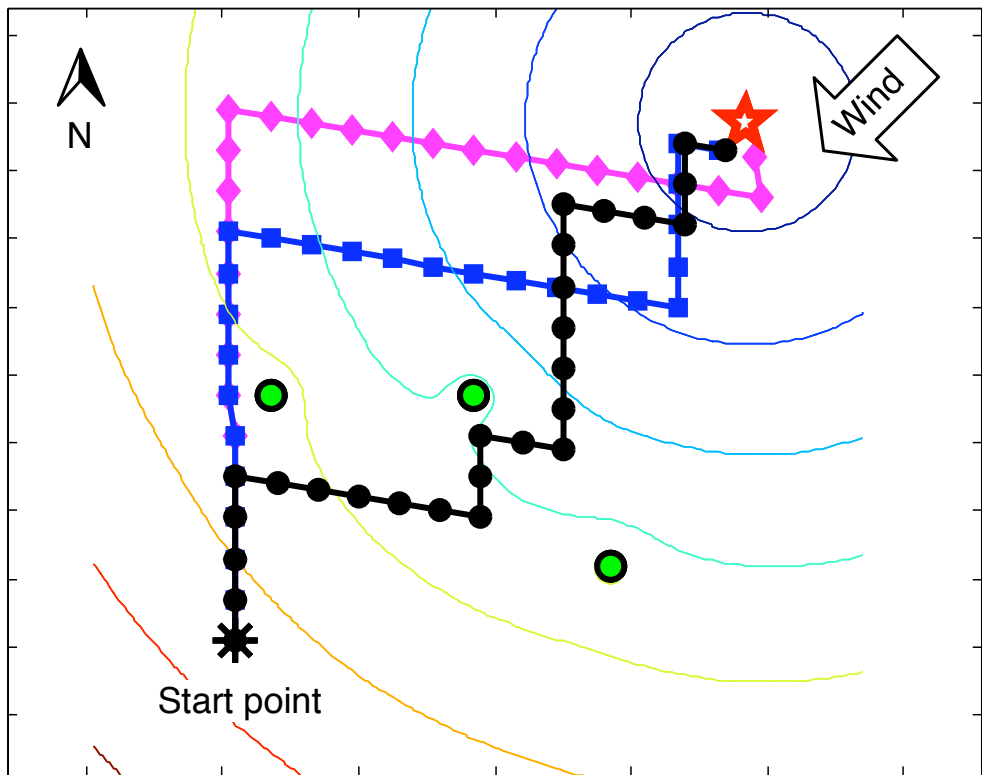


Fig. 13. Upwind navigation with obstacles: influence of the hysteresis potential value

B. Experimental results

Experiments have been conducted on a lake near Nantes (France) using our sailboat prototype (see Fig. 1). The purpose of these experiments¹ was to test the navigation and control modules of the sailboat, without the obstacle detection module.

For the field test depicted in figure 14, the mean wind angle in the NED (North-East-Down) reference frame was 330° with a standard deviation of 13° . The true wind speed was equal to 5.3 m/s (mean value) with a standard deviation of 0.8 m/s and the boat speed was 1.3 m/s (mean value, standard deviation: 0.3 m/s). All the data during this run was logged at a sampling frequency of 10 Hz , which is equal to the running frequency of the low level control loop and local path planner algorithm.

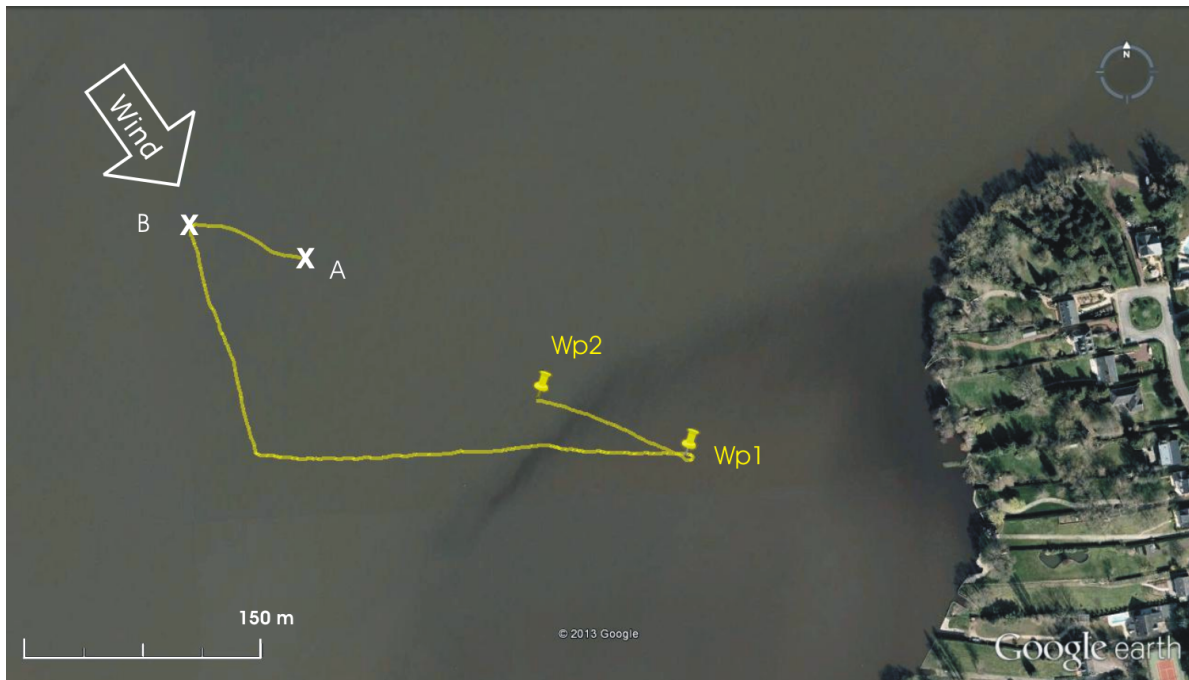


Fig. 14. Field experiments: GPS trace for downwind navigation

For this run, the sailboat is first manually controlled using the gamepad from point A to point B. At point B, the control mode is switched to autonomous mode with the goal set to the first

¹The authors wish to thank J.M. Rousset and his team from the Hydrodynamics, Energetics and Atmospheric Environment laboratory of Ecole Centrale de Nantes for their help during the field tests of the sailboat in Nantes.

way point Wp_1 . Since the direct route between point B and the current goal Wp_1 lies in the downwind no-go zone, the local path planner of the embedded navigation module computes a feasible heading (180° in the NED frame, 210° with respect to the wind), outside of the no-go zone. After one gybe, the sailboat reaches the goal Wp_1 and sails to the next waypoint Wp_2 . The desired heading (computed in real time by the local path planner), the real heading and the measured wind direction (all in the NED frame) are depicted in figure 15.

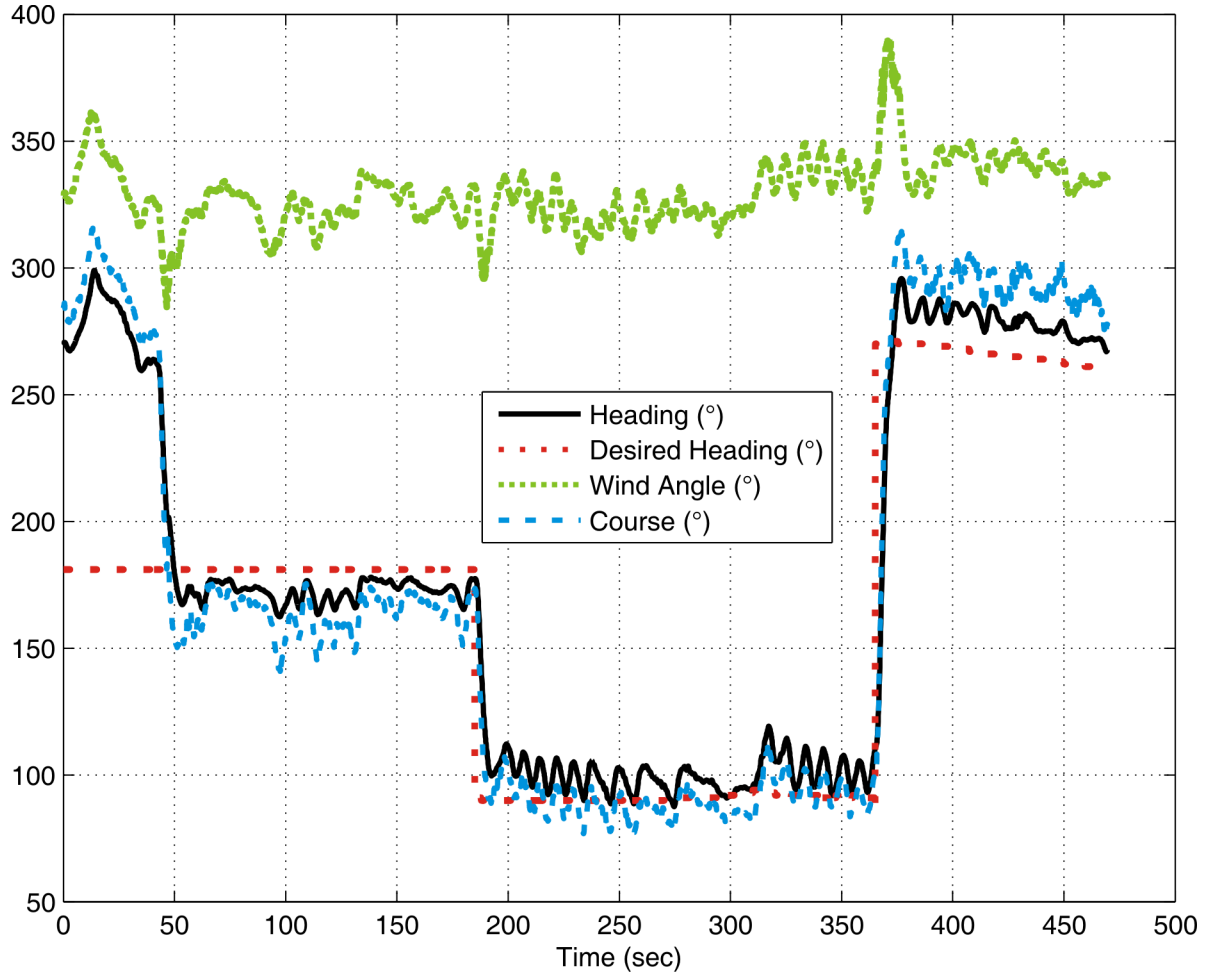


Fig. 15. Field experiments: Heading, course and wind direction

The course (direction of the sailboat velocity vector) is also shown in this figure, with a mean drift (leeway angle) of around 10° with respect to the heading (yaw angle of the vehicle).

The desired and measured heading with respect to the wind direction are depicted in figure

16. As expected, one can see that the desired heading from point *B* to the first gybe maneuver was set to the limit of the downwind no-go zone (210° , see §II-B) thanks to the virtual repulsive potential associated to the downwind no-go zone.

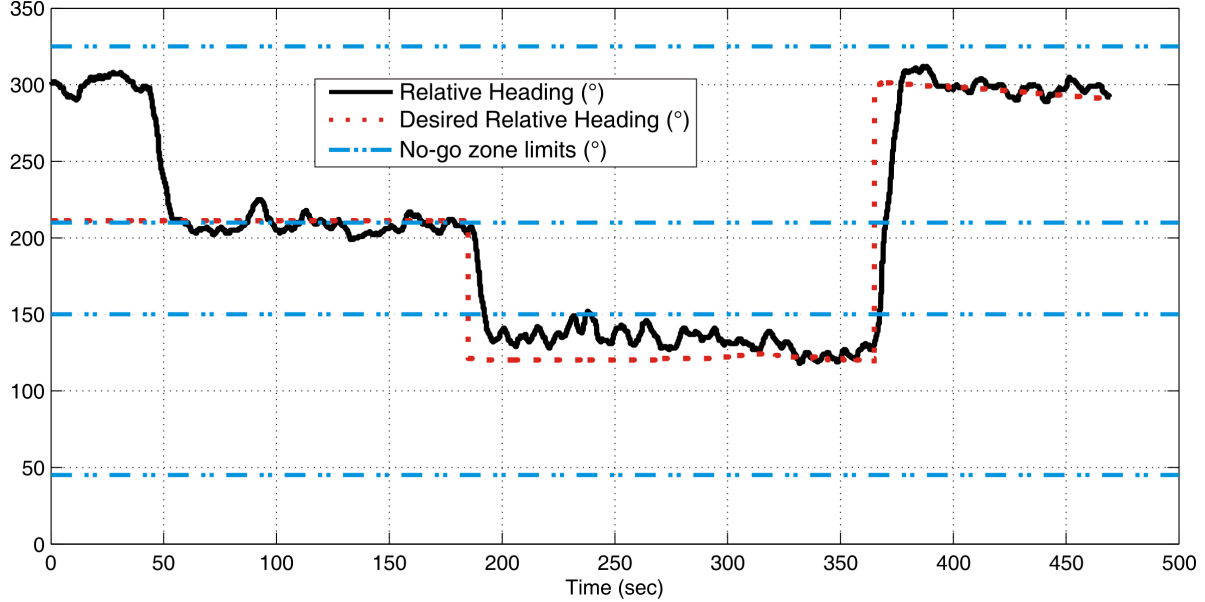


Fig. 16. Field experiments: Heading and no-go zones

Figure 17 shows the two low level control inputs: the mainsail angle and the rudder angle. During this field test, the desired sail angle was kept constant (30° regardless of the wind direction) since the speed optimization was not the objective in this case. The rudder PD controller was only active when the heading error was greater than an empirically sets value of 7° . This allows a power consumption reduction since, in this case the rudder actuator is only active 10% of the time which is two times less than the value used for the estimation of the power budget briefly outlined in section II-A. Of course, this comes at the expense of the accuracy of the heading control and can explain the heading oscillations of the sailboat.

V. CONCLUSION

In this work, a global architecture for a sailing robot has been presented. The use of a set of sensors and actuators combined with solar and wind energy harvesting will achieve the challenging task of giving autonomy to these kind of surface vehicle: energy autonomy as well

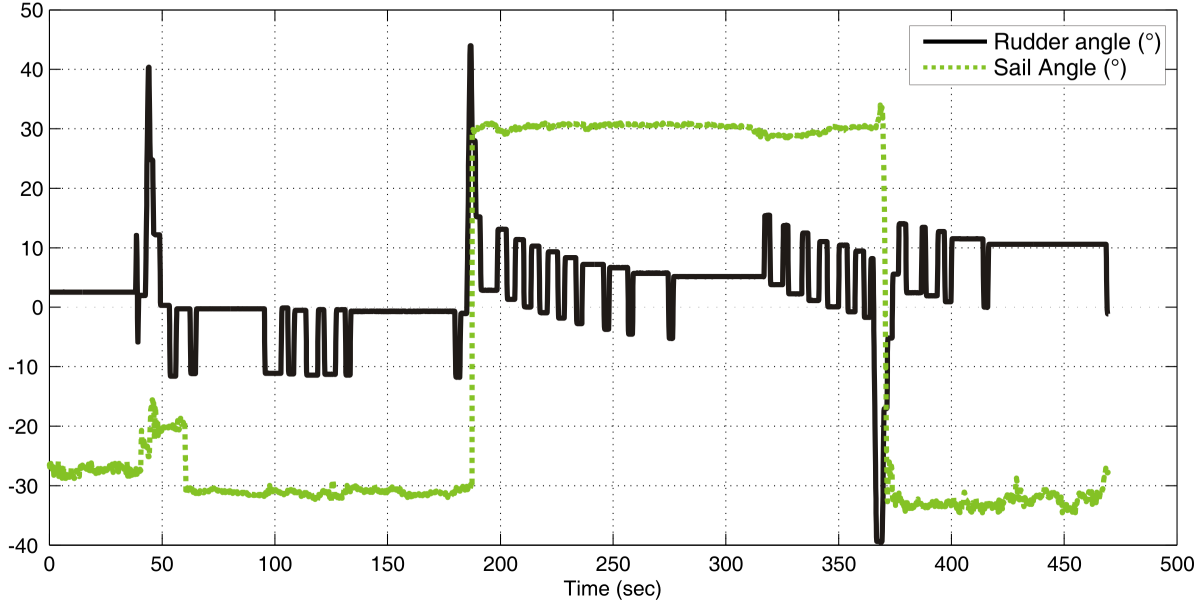


Fig. 17. Field experiments: Rudder and sail angles

as decision-making autonomy, under variable and possibly dangerous navigation conditions. Perception, navigation and control modules are in charge of the sailing autonomy of the robot. Visual, acoustic and inertial data are used to address the critical task of detecting and localizing the surrounding obstacles. A new potential field approach has been proposed for the navigation task, which respects the specific kinematics constraints of sailing boats. Unit tests were performed for each of these aforementioned features and constitute the first steps toward a fully autonomous and functional sailing robot.

REFERENCES

- [1] J. Manley, "Unmanned surface vehicles, 15 years of development," in *MTS/IEEE OCEANS 2008*, 2008.
- [2] M. Robin, S. Eric, G. Chandler, C. Charlie, H. Mike, and P. Kevin, "Cooperative use of unmanned sea surface and micro aerial vehicles at hurricane wilma," *Journal of Field Robotics*, vol. 25, no. 3, pp. 164–180, 2008.
- [3] T. Pastore and V. Djapic, "Improving autonomy and control of autonomous surface vehicles in port protection and mine countermeasure scenarios," *Journal of Field Robotics*, vol. 27, no. 6, pp. 903–914, 2010.
- [4] P. Mahacek, T. Berk, A. Casanova, C. Kitts, W. Kirkwood, and G. Wheat, "Development and initial testing of a swath boat for shallow-water bathymetry," in *MTS/IEEE OCEANS 2008*, 2008.

- [5] E. Steimle and M. Hall, "Unmanned surface vehicles as environmental monitoring and assessment tools," in *MTS/IEEE OCEANS 2006*, 2006.
- [6] P. Mahacek, R. Kobashigawa, A. Schooley, and C. Kitts, "The wasp: an autonomous surface vessel for the university of alaska," in *MTS/IEEE OCEANS 2005*, 2005, pp. 2282 – 2291 Vol. 3.
- [7] M. Caccia, R. Bono, G. Bruzzone, E. Spirandelli, G. Veruggio, A. Stortini, and G. Capodaglio, "Sampling sea surfaces with sesamo: an autonomous craft for the study of sea-air interactions," *IEEE Robotics Automation Magazine*, vol. 12, no. 3, pp. 95 – 105, 2005.
- [8] A. Pascoal, P. Oliveira, C. Silvestre, and et al, "Robotic ocean vehicles for marine science applications: the european asimov project," in *MTS/IEEE OCEANS 2000*, 2000, pp. 409–415 vol.1.
- [9] A. Dhariwal and G. Sukhatme, "Experiments in robotic boat localization," in *IEEE/RSJ Int. Conf. on Intelligent Robots and Systems*, 2007, pp. 1702 –1708.
- [10] G. Podnar, J. Dolan, A. Elfes, S. Stancliff, E. Lin, J. Hosier, T. Ames, J. Moisan, T. Moisan, J. Higinbotham, and E. Kulczycki, "Operation of robotic science boats using the telesupervised adaptive ocean sensor fleet system," in *IEEE Int. Conf. on Robotics and Automation*, 2008, pp. 1061 –1068.
- [11] J. Curcio, J. Leonard, and A. Patrikalakis, "Scout - a low cost autonomous surface platform for research in cooperative autonomy," in *MTS/IEEE OCEANS 2005*, 2005, pp. 725 – 729 Vol. 1.
- [12] D. Eickstedt, M. Benjamin, H. Schmidt, and J. Leonard, "Adaptive control of heterogeneous marine sensor platforms in an autonomous sensor network," in *IEEE/RSJ Int. Conf. on Intelligent Robots and Systems*, 2006, pp. 5514 –5521.
- [13] N. Cruz and J. Alves, "Autonomous sailboats: An emerging technology for ocean sampling and surveillance," in *MTS/IEEE OCEANS 2008*, 2008.
- [14] P. Rynne and K. von Ellenrieder, "A wind and solar-powered autonomous surface vehicle for sea surface measurements," in *OCEANS 2008*, 2008.
- [15] Y. Briere, "IBoat: an unmanned sailing robot for the Microtransat challenge and ocean monitoring," in *Conf. TAROS (Towards Autonomous Robotic Systems)*, 2007, pp. 145–162.
- [16] C. Petres, M. Romero Ramirez, F. Plumet, and B. Alessandrini, "Modeling and reactive navigation of an autonomous sailboat," in *IEEE/RSJ International Conference on Intelligent RObots and Systems (IROS)*, 2011, pp. 3571–3576.
- [17] X. Gong, "Omnidirectional vision for an autonomous surface vehicle," Ph.D. dissertation, Faculty of the Virginia Polytechnic Institute and State University, 2008.
- [18] A. Martin, E. An, K. Nelson, and S. Smith, "Obstacle detection by a forward looking sonar integrated in an autonomous underwater vehicle," in *MTS/IEEE OCEANS 2000*, 2000, pp. 337–341 vol.1.
- [19] S. Zhao, "Automatic underwater multiple objects detection and tracking using sonar imaging," Ph.D. dissertation, University of Adelaide, South Australia, 2010.
- [20] I. Quidu, A. Hetet, Y. Dupas, and S. Lefevre, "Auv (redermor) obstacle detection and avoidance experimental evaluation," in *MTS/IEEE OCEANS 2007*, 2007.
- [21] S. Majumder, S. Scheding, and H. F. Durrant-Whyte, "Multisensor data fusion for underwater navigation," *Robotics and Autonomous Systems*, vol. 35, no. 2, pp. 97–108, 2001.
- [22] Y. Guo, M. Romero, S.-H. Ieng, F. Plumet, R. Benosman, and B. Gas, "Reactive path planning for autonomous sailboat using an omni-directional camera for obstacle detection," in *IEEE International Conference on Mechatronics*, 2011.
- [23] M. Neal, "A hardware proof of concept of a sailing robot for ocean observation," *IEEE Journal of Oceanic Engineering*, vol. 31, no. 2, 2006.

- [24] R. Stelzer and T. Proll, "Autonomous sailboat navigation for short course racing," *Robotics and Autonomous Systems*, vol. 56, no. 7, pp. 604 – 614, 2008.
- [25] Y. Briere, F. L. Cardoso Ribeiro, and M. Vieira Rosa, "Design methodologies for the control of an unmanned sailing robot," in *8th Conf. on Manoeuvring and Control of Marine Craft*, 2009.
- [26] G. Elkaim and C. Boyce, "Energy scavenging and aerodynamic performance of a rigid wing propulsion system for an autonomous surface vessel," in *ION Global Navigation Satellite Systems Conference*, 2009.
- [27] H. Erckens, G.-A. Busser, C. Pradalier, and R. Siegwart, "Avalon: Navigation strategy and trajectory following controller for an autonomous sailing vessel," *IEEE Robotics Automation Magazine*, vol. 17, no. 1, pp. 45 –54, 2010.
- [28] J. Abril, J. Salom, and O. Calvo, "Fuzzy control of a sailboat," *International Journal of Approximate Reasoning*, vol. 16, pp. 359–375, 1997.
- [29] C. Sauze and M. Neal, "A neuro-endocrine inspired approach to long term energy autonomy in sailing robots," in *Proc. TAROS 2010 : Towards Autonomous Robotic Systems*, 2010.
- [30] R. Stelzer, K. Jafarmadar, H. Hassler, and R. Charwot, "A reactive approach to obstacle avoidance in autonomous sailing," in *3rd Int. Robotic Sailing Conference*, 2010.
- [31] O. Khatib, "Real-time obstacle avoidance for manipulators and mobile robots," *International Journal of Robotics Research*, vol. 5, no. 1, pp. 90–98, 1986.
- [32] B. Krogh and C. Thorpe, "Integrated path planning and dynamic steering control for autonomous vehicles," in *IEEE Int. Conf. on Robotics and Automation*, vol. 3, 1986, pp. 1664–1669.
- [33] J. Barraquand, B. Langlois, and J.-C. Latombe, "Numerical potential field techniques for robot path planning," *IEEE Transactions on Systems, Man and Cybernetics*, vol. 22, no. 2, pp. 224 –241, 1992.
- [34] H. Haddad, M. Khatib, S. Lacroix, and R. Chatila, "Reactive navigation in outdoor environments using potential fields," in *IEEE Int. Conf. on Robotics and Automation*, vol. 2, 1998, pp. 1232 –1237.
- [35] S. Ge and Y. Cui, "Dynamic motion planning for mobile robots using potential field method," *Autonomous Robots*, vol. 13, no. 3, pp. 207 –222, 2002.
- [36] S. Shimoda, Y. Kuroda, and K. Iagnemma, "Potential field navigation of high speed unmanned ground vehicles on uneven terrain," in *IEEE Int. Conf. on Robotics and Automation*, 2005, pp. 2828 – 2833.